Appl Compos Mater (2014) 21:227–245
DOI 10.1007/s10443-013-9363-2

Dynamic Responses of Composite Structures in Contact with Water While Subjected to Harmonic Loads

Y. W. Kwon

Received: 13 September 2013 / Accepted: 11 November 2013 / Published online: 18 December 2013

Abstract Composite ship hull structures are in contact with water on the external surfaces and may support vibrating equipment on the internal surfaces. This study examined how the Fluid-structure Interaction (FSI) coupled with the harmonic excitation could affect the composite structural response. A multiphysics computational technique based on the Finite Element Method (FEM) and Cellular Automata (CA) was developed and applied for this research. A comparison was made on the structural responses with and without FSI for composite beams and plates. Furthermore, metallic structures made of either aluminum or steel were also compared to composite structures to investigate the effect of the coupled FSI and a harmonically vibrating machine. The study showed that FSI could magnify the displacement and stress level in composite structures supporting harmonically vibrating equipment. Analysis of composite structures supporting such equipment without considering the FSI effect would result in non-conservative design leading to pre-mature failure. A parametric study was conducted to determine what parameter could signify the FSI effect on composite structures.

Keywords Fluid-structure interaction · Vibrating equipment · Multiphysics analysis

1 Introduction

When a device or equipment is attached to a base structure, and either the device or the base structure is subjected to a dynamic load such as shock or vibration; it is desirable to reduce the transmission of unwanted vibration and shock from the excited one to the other. In that regards, extensive research has been conducted for shock and vibration as well as its isolation [1–6].

The naval structures such as ships have the same kind of problems because the ship structures support many vibrating equipment [7]. If a ship is subjected to a dynamic loading such as water slamming or underwater explosion [8–10], the equipment on board should be protected from the ship structural dynamic response [11]. On the other hand, it is necessary to minimize the ship structural response from the vibrating equipment.

Y. W. Kwon (✉)
Department of Mechanical & Aerospace Engineering, Naval Postgraduate School, Monterey, CA 93943, USA
e-mail: ywkwon@nps.edu

The ship structure has one additional characteristic. Because the ship hull is in contact with water, Fluid-structure Interaction (FSI) plays an important role [12–14]. As polymer composite materials have been used increasingly for ship structures, the effect of FSI becomes much more significant for composite structures because their densities are comparable to the water density. Sandwich composite structures constructed of very light core materials may have a lower density than water. Therefore, the effect of FSI on composite structures has been investigated recently [15–18]. In those studies, impact loading was applied to polymer composite structures, and both experimental and numerical studies were conducted. Those studies showed the effect of FSI was detrimental and contributed to the damage and failure of composite structures. Furthermore, the experimental modal analysis conducted in Ref. [18] suggested that not only vibrational frequency but also mode shape, especially modal curvature, were affected by FSI.

The objective of this study is to examine the dynamic responses of polymer composite structures which are in contact with water on one side and support vibrating equipment on the other side. Numerical analyses were undertaken using the multiphysics modeling. The Finite Element Method (FEM) was applied to the structural medium while coupled FEM and Cellular Automata (CA) [17,19] were applied to the fluid medium. Structures were analyzed using 3-D solid-like shell elements [20] which have the 3-D geometry and displacement degrees of freedom at nodes but no rotational degree of freedom. These shell elements are easy to be coupled with the fluid analyzer at the interface of the fluid-structure media. Furthermore, the combined FEM and CA technique was utilized for the fluid medium because the combined method is computationally efficient and easy to model any kind of boundary condition and shape, as discussed in further details later.

The next section describes the problem to be studied, followed by the formulations for structural analysis as well as the fluid domain analysis. Then, numerical examples are presented and discussed. Finally conclusions are provided at the end.

2 Problem Description

A composite structure supports vibrating equipment on its top side and is in contact with water on the bottom side as sketched in Fig. 1. The water domain is considered as a semi-infinite domain. The corresponding engineering model is presented in Fig. 2 with detailed explanations below.

The vibrating equipment was simplified as a single mass and a spring with a harmonic motion. The damping was neglected in the model. Neglecting damping would not affect the objective of the present study because the structural response was compared with and without the FSI effect under the same condition otherwise. Furthermore, neglecting damping results in

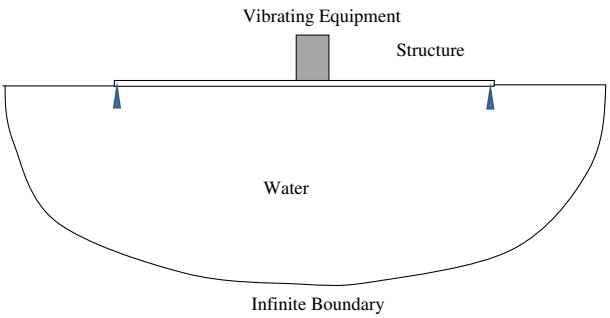

Fig. 1 Structure supporting vibrating equipment while being in contact with water

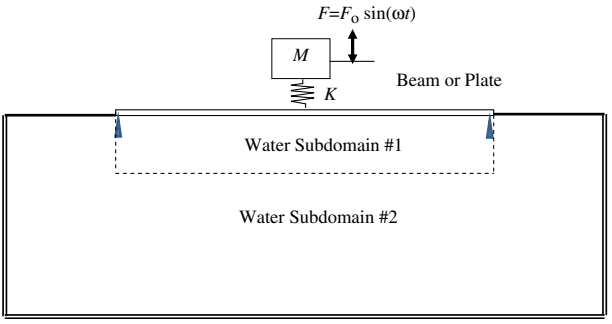

Fig. 2 Engineering model to represent a structure supporting vibrating equipment while being in contact with water

more severe vibrations. Therefore, damping was omitted in this study. The vibration of the equipment was modeled as a harmonic force applied to the mass.

The structure was modeled as a beam or a plate depending on the structural dimensions. Both cases were considered here, respectively. The finite element method was used to solve the dynamic response of the beam or plate. Because the beam or plate must be coupled with the fluid, i.e., water, the beam or plate finite elements were formulated to have only displacement degrees of freedom at each node like a 3-D solid element. This makes the compatibility at the fluid-structural interface easy. The detailed formulations for the structural analysis are provided at a later section. The boundary of the structure was either simply supported or clamped.

Some assumptions were made for the water medium for simplicity. Viscosity and flow motion were neglected such that the fluid medium can be modeled as an acoustic medium represented by the wave equation. Then, the water domain was broken into two subdomains as shown by broken lines in Fig. 2 in order to achieve the computational efficiency as well as easy compatibility at the fluid-structure interface as described in more detail later. The water subdomain #1 was analyzed using FEM while the water subdomain #2 was solved using CA. The top boundary of the water domain, represented by thick solid lines, is free while the other boundary, denoted by double solid lines, are non-reflective boundary like an infinite boundary. Both boundary conditions can be easily represented by CA. Additionally both water subdomains were properly coupled to have continuity of the solution.

As a harmonic force was applied to the single mass, the dynamic response of the structure was analyzed. The structure may or may not be in contact with water during the harmonic excitation. The results from the two cases were compared to study the effect of FSI. A series of parametric studies were undertaken by changing parameters such as the vibrational frequency, boundary condition, structural materials, etc.

3 Formulation for Structural Analysis

The structure was modeled as a beam or a plate using FEM. This section describes the finite element formulations for the structural elements used in this study. A 3-D solid like shell element [20] was utilized because the element is easy to couple with the acoustic element used for modeling the water medium as discussed later. The beam and plate elements are simplified cases of the shell element. As a result, the shell element formulation is presented below.

The shell element is like a 3-D solid element such that the shell is modeled as a 3-D geometry rather than a 2-D plane geometry. Therefore, the shell element has multiple nodes through the shell thickness. Each node has three translational degrees of freedom but not rotational degrees of

freedom. As a result, the shell element looks the same as 3-D solid elements except that the shell element can have a much smaller dimension in the thickness direction compared to inplane dimensions. The shell element is sketched in Fig. 3(a) in terms of both local and global coordinate systems. The local coordinate is attached to the shell element. Two local axes are tangential to the shell plane while the third local axis is normal to the shell plane. The degenerated beam element is shown in Fig. 3(b). For the beam, the first local axis is along the beam, and the second local axis is along the beam thickness, and the third local axis is perpendicular to the other two local axes. The shell element shown in the figure has eight nodes while the beam element has four nodes. Higher order elements can be also developed. However, the present study used only eight-node shell and four-node beam elements. The following development is for the shell element.

The displacements in the local coordinate system are expressed as

$$u(x,y,z) = \sum_{i=1}^{n_1}\sum_{j=1}^{n_2} N_i(\xi,\eta)H_j(\zeta)u_{ij} \tag{1}$$

$$v(x,y,z) = \sum_{i=1}^{n_1}\sum_{j=1}^{n_2} N_i(\xi,\eta)H_j(\zeta)v_{ij} \tag{2}$$

$$w(x,y,z) = \sum_{i=1}^{n_1}\sum_{j=1}^{n_2} N_i(\xi,\eta)H_j(\zeta)w_{ij} \tag{3}$$

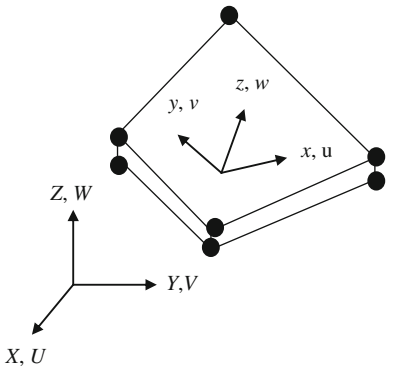

(a) Shell element

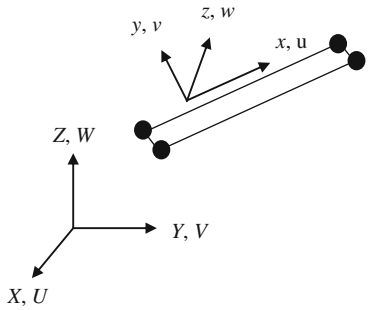

(a) Beam element

Fig. 3 Shell and beam elements in terms of local and global coordinate systems

where $N_i(\xi,\eta)$ is the 2-D shape function for the inplane interpolation while $H_j(\varsigma)$ is the 1-D shape function for the transverse interpolation. Here, (ξ,η,ς) is the natural coordinate system associated with the isoparametric shape functions N_i and H_j.

The strain components are divided into three parts, inplane strains, transverse shear strains, and the transverse normal strain. The inplane strains in terms of the shell local coordinate system are expressed as

$$\{\varepsilon_{inpl}\} = \begin{Bmatrix} \varepsilon_x \\ \varepsilon_y \\ \gamma_{xy} \end{Bmatrix} = \begin{bmatrix} \frac{\partial}{\partial x} & 0 & 0 \\ 0 & \frac{\partial}{\partial y} & 0 \\ \frac{\partial}{\partial y} & \frac{\partial}{\partial x} & 0 \end{bmatrix} \begin{Bmatrix} u \\ v \\ w \end{Bmatrix} \tag{4}$$

while the transverse shear strains are given by

$$\{\varepsilon_{tranv}\} = \begin{Bmatrix} \gamma_{xz} \\ \gamma_{yz} \end{Bmatrix} = \begin{bmatrix} \frac{\partial}{\partial z} & 0 & \frac{\partial}{\partial x} \\ 0 & \frac{\partial}{\partial z} & \frac{\partial}{\partial y} \end{bmatrix} \begin{Bmatrix} u \\ v \\ w \end{Bmatrix} \tag{5}$$

Additionally, the transverse normal strain is shown as

$$\varepsilon_z = \frac{\partial w}{\partial z} \tag{6}$$

Substitution of Eqs. (1) through (3) into Eq. (4) yields the expression for the inplane strains in terms of nodal displacements.

$$\{\varepsilon_{inpl}\} = [B_b]\{d_{local}\} \tag{7}$$

where

$$[B_b] = [\, B_{b1} \quad B_{b2} \,] \tag{8}$$

$$[B_{bi}] = \begin{bmatrix} H_i\frac{\partial N_1}{\partial x} & 0 & 0 & H_i\frac{\partial N_2}{\partial x} & 0 & 0 & H_i\frac{\partial N_3}{\partial x} & 0 & 0 & H_i\frac{\partial N_4}{\partial x} & 0 & 0 \\ 0 & H_i\frac{\partial N_1}{\partial y} & 0 & 0 & H_i\frac{\partial N_2}{\partial y} & 0 & 0 & H_i\frac{\partial N_3}{\partial y} & 0 & 0 & H_i\frac{\partial N_4}{\partial y} & 0 \\ H_i\frac{\partial N_1}{\partial y} & H_i\frac{\partial N_1}{\partial x} & 0 & H_i\frac{\partial N_2}{\partial y} & H_i\frac{\partial N_2}{\partial x} & 0 & H_i\frac{\partial N_3}{\partial y} & H_i\frac{\partial N_3}{\partial x} & 0 & H_i\frac{\partial N_4}{\partial y} & H_i\frac{\partial N_4}{\partial x} & 0 \end{bmatrix} \tag{9}$$

$$\{d_{local}\}^T = \{\, d_1 \quad d_2 \quad d_3 \quad d_4 \quad d_5 \quad d_6 \quad d_7 \quad d_8 \,\} \tag{10}$$

$$\{d_i\} = \{\, u_i \quad v_i \quad w_i \,\} \tag{11}$$

The first four nodes in Eq. (10) are on the bottom of the shell element while the last four nodes are on the top of the element. Likewise, the transverse shear strains in terms of the nodal displacements are expressed as

$$\{\varepsilon_{trans}\} = [B_s]\{d_{local}\} \tag{12}$$

where

$$[B_s] = [\, B_{s1} \quad B_{s2} \,] \tag{13}$$

$$[B_{si}] = \begin{bmatrix} N_1\frac{\partial H_1}{\partial z} & 0 & H_1\frac{\partial N_1}{\partial x} & N_2\frac{\partial H_1}{\partial z} & 0 & H_1\frac{\partial N_2}{\partial x} & N_3\frac{\partial H_1}{\partial z} & 0 & H_1\frac{\partial N_3}{\partial x} & N_4\frac{\partial H_1}{\partial z} & 0 & H_1\frac{\partial N_4}{\partial x} \\ 0 & N_1\frac{\partial H_1}{\partial z} & H_1\frac{\partial N_1}{\partial y} & 0 & N_2\frac{\partial H_1}{\partial z} & H_1\frac{\partial N_2}{\partial y} & 0 & N_3\frac{\partial H_1}{\partial z} & H_1\frac{\partial N_3}{\partial y} & 0 & N_4\frac{\partial H_1}{\partial z} & H_1\frac{\partial N_4}{\partial y} \end{bmatrix} \tag{14}$$

The transverse normal strain can be expressed in a similar manner.

The element stiffness matrix with respect to the shell local coordinate system consists of the three parts; inplane bending energy, transverse shear energy, and transverse normal energy as expressed below

$$[K_{local}] = \int_{\Omega^e} [B_b]^T [D_b][B_d] d\Omega + \int_{\Omega^e} [B_s]^T [D_s][B_s] d\Omega + \int_{\Omega^e} [B_z]^T D_z [B_z] d\Omega \tag{15}$$

The vector $[B_z]$ can be easily obtained by substitution of Eq. (3) into Eq. (6). Furthermore, $[D_b]$ and $[D_s]$ are the material property matrices for the bending and transverse shear terms. If the elastic modulus D_z is selected as an arbitrary large number, the third term in Eq. (15) is equivalent to applying the penalty method for the transverse displacements. In order to prevent transverse shear locking, the second term is integrated using a reduced integration technique.

The final step is to apply the coordinate transformation from the local axes to the global axes so that every element stiffness matrix can be assembled properly. Let (l_1, m_1, n_1) be the direction cosines between x- and X-axis, (l_2, m_2, n_2) be the direction cosines between y- and Y-axis, and (l_3, m_3, n_3) be the direction cosines between z- and Z-axis.

The compatibility of displacements between the two coordinate systems requires

$$\begin{Bmatrix} \frac{u^i + u^{i+4}}{2} \\ \frac{v^i + v^{i+4}}{2} \\ \frac{w^i + w^{i+4}}{2} \end{Bmatrix} = \begin{bmatrix} l_1 & m_1 & n_1 \\ l_2 & m_2 & n_2 \\ l_3 & m_3 & n_3 \end{bmatrix} \begin{Bmatrix} \frac{U^i + U^{i+4}}{2} \\ \frac{V^i + V^{i+4}}{2} \\ \frac{W^i + W^{i+4}}{2} \end{Bmatrix} \tag{16}$$

and

$$\begin{Bmatrix} u^{i+4} - u^i \\ v^{i+4} - v^i \\ w^{i+4} - w^i \end{Bmatrix} = \begin{Bmatrix} U^{i+4} - U^i \\ V^{i+4} - V^i \\ W^{i+4} - W^i \end{Bmatrix} \tag{17}$$

where the superscript 'i' denotes the node from 1 to 4 in Fig. 2. Solving the two set of equations results in

$$\begin{Bmatrix} u^i \\ v^i \\ w^i \\ u^{i+4} \\ v^{i+4} \\ w^{i+4} \end{Bmatrix} = \frac{1}{2} \begin{bmatrix} l_1 + 1 & m_1 & n_1 & l_1 - 1 & m_1 & n_1 \\ l_2 & m_2 + 1 & n_2 & l_2 & m_2 - 1 & n_2 \\ l_3 & m_3 & n_3 + 1 & l_3 & m_3 & n_3 - 1 \\ l_1 - 1 & m_1 & n_1 & l_1 + 1 & m_1 & n_1 \\ l_2 & m_2 - 1 & n_2 & l_2 & m_2 + 1 & n_2 \\ l_3 & m_3 & n_3 - 1 & l_3 & m_3 & n_3 + 1 \end{bmatrix} \begin{Bmatrix} U^i \\ V^i \\ W^i \\ U^{i+4} \\ V^{i+4} \\ W^{i+4} \end{Bmatrix} \tag{18}$$

Applying this relation to all sets of nodal displacements yields the following equation:

$$\{d_{local}\} = [T]\{d_{global}\} \tag{19}$$

Then, the element stiffness matrix in terms of the global coordinate system is expressed as

$$[K_{global}] = [T]^T [K_{local}][T] \tag{20}$$

4 Formulation for Fluid Analysis

In order to simplify the fluid domain, it was assumed that the fluid flow and viscosity were negligible. As a result, the fluid domain was modeled as an acoustic domain. In that aspect, the wave equation is used to solve the fluid medium. The wave equation can be expressed in terms of many different variables such as pressure, velocity potential, etc. In this study, the velocity ϕ is selected such that the wave equation is

$$c^2\nabla^2\phi = \frac{\partial^2\phi}{\partial t^2} = \ddot{\phi} \tag{21}$$

where c is the acoustic speed of the medium, and the velocity is expressed as

$$\overrightarrow{v} = \nabla\phi \tag{22}$$

The wave equation can be solved using different computational techniques. However, the CA is one of the most efficient computational methods. Cellular Automata are discrete, rule-based numerical methods that can model complex physical phenomena with relative simplicity. Generally, both the space and time are treated discretely and the value of the quantity in question is limited to a finite set of values. As the space-time domain proceeds or grows, the seemingly simple model converges to the complex real-world behavior. The simplicity of the chosen rules and their implementation lowers the computational cost while still achieving the required accuracy.

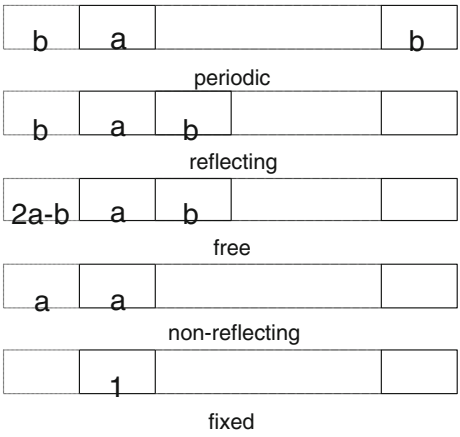

Fig. 4 Virtual cell values for various boundary conditions in one dimension of CA

Table 1 Material properties

	Elastic modulus (GPa)	Density (Kg/m^3)
E-glass composite	20	2000
Aluminum	70	2700
Steel	200	8000

Following the work in ref. [17], the wave equation in the three-dimension uses the following rules:

$$\phi_c(t+\Delta t) = \frac{1}{3}(\phi_w(t) + \phi_E(t) + \phi_S(t) + \phi_N(t) + \phi_F(t) + \phi_B(t) - 3\phi_c(t-\Delta t)) \quad (23)$$

The value of ϕ at each interior grid point in the domain of interest (ϕ_c) is updated according to the values at its nearest neighbors. Subscripts '*W*', '*E*', '*S*', '*N*, '*F*', and '*B*' denote west, east, south, north, front, and back with respect to ϕ_c. All grid points are divided into two sets, "black" and "white" (or "odd" and "even"), such that the neighbors of each white point are all black, and only one "color" is updated during each iteration. Furthermore, Δt is the time increment which depends on the grid size and the wave speed, and it is expressed as

$$\Delta t = \frac{\Delta x}{c\sqrt{n_{\text{dim}}}} \quad (24)$$

where Δx is the grid space, c is the wave speed, and n_{dim} is the dimension of the problem

Another useful advantage of the CA technique is that it can easily model various boundary conditions such as the non-reflected boundary, free boundary, periodic boundary, fixed boundary, etc. How to apply such boundary condition to CA is sketched in Fig. 4 for the 1-D domain, which can be extended to 2-D and 3-D domains very easily.

One of the drawbacks of the CA technique is that it uses grids of a square shape in 2-D and a cube shape in 3-D. As a result, the technique requires very fine grids to approximate a curved boundary. Additionally, at the interface of the structure and fluid domains, the velocity and pressure should be computed at the interface boundary from both media in order to maintain the interface compatibility. The velocity and pressure in the fluid medium are computed from the spatial and temporal derivatives of the velocity potential. Because the CA technique updates the velocity potential at the grids alternately, i.e., either black or white grids as described previously, applying the finite difference technique to compute the velocity and pressure at the interface boundary does not yield acceptable solutions.

In order to overcome this difficulty, a mixed solution technique was developed [7,9]. Around a fluid-structure interface boundary or a curved boundary, the finite element formulation for the wave equation was applied. Because the FEM is computationally much more expensive than the CA technique, the finite element domain is only limited to a necessary local

Table 2 First natural frequencies of beams in air

	Clamped	Simply supported
E-glass composite	65.09 Hz	28.68 Hz
Aluminum	104.8 Hz	47.18 Hz
Steel	102.9 Hz	45.35 Hz

domain, and the rest of the fluid domain is modeled using the CA technique. Combination of the FEM and CA techniques for the fluid medium solves the short-comings of each technique so that they are computationally efficient and can be applied to any kind of boundary.

The interface of the FEM and CA subdomains of the fluid medium is handled in the following way. The general idea is to have a small number of multiple layers of finite elements in contact with the structure and then to have that fluid volume surrounded with a CA subdomain upon which the non-reflecting and free boundary conditions can be imposed as shown in Fig. 2, where the water subdomain #1 is modeled using FEM and the water subdomain #2 is modeled using CA. The two fluid domains will interact such that the outer layer of finite element nodes will be processed as interior CA nodes whose CA-calculated values become FE-specified boundary values. The next set of FE nodes inside the domain are calculated by the FE machinery and then passed to the CA domain to serve as neighbors for application of the CA rule to the outer set.

5 Results and Discussion

First, a beam structure was analyzed. The beam was made of a composite, aluminum, or steel, respectively. Their material properties are listed in Table 1. In order to avoid the resonance effect, the frequency of the vibration equipment was selected much lower than the natural frequencies of the structures. The beam was assumed to be 1.0 m long, 0.1 m wide and 0.02 m thick. Then, the first natural frequency of the beam is listed in Table 2 for all three different materials with the given geometric data. The composite beam has the lowest frequency of 65 Hz for the clamped boundaries at both ends. This is the frequency in air, i.e., without the effect of water. Additionally, the natural frequency of the clamped composite beam including the additional single mass and spring as shown in Fig. 2 was computed using the FEM. The mesh sensitivity study showed that using 20 or more beam elements resulted in consistent first several natural frequencies. The frequencies depend on the spring-to-mass ratio, $\sqrt{K/M}$. Figure 5 shows the first natural frequency of the clamped composite beam with the centrally attached mass and spring (called a beam system from now on) as a function of the spring-to-mass ratio, $\sqrt{K/M}$. The graph is almost linear up to the ratio of $\sqrt{K/M} = 1000$ (rad/sec).

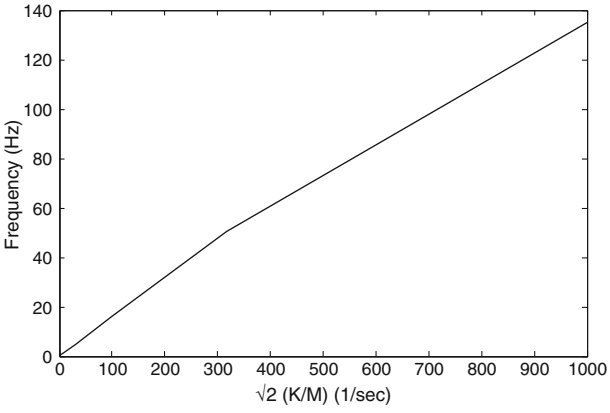

Fig. 5 Plot of first natural frequency of clamped composite beam in air with centrally attached mass and spring as a function of the spring-to-mass ratio

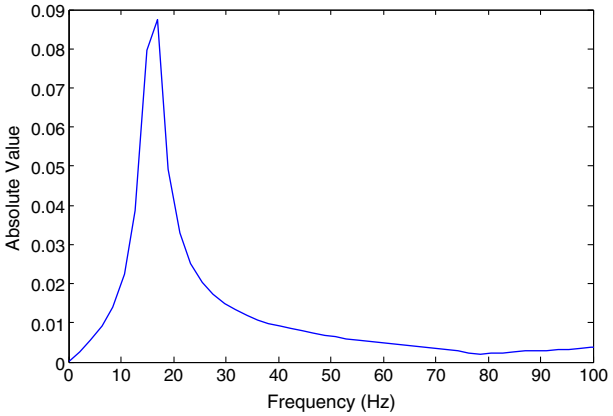

Fig. 6 FFT plot of clamped composite beam submerged in water

This suggests the first natural frequency of the beam system varies almost linearly with the ratio of $\sqrt{K/M}$. When the ratio $\sqrt{K/M}$ is approximately less than 500 (rad/sec), the first natural frequency of the clamped composite beam system is smaller than that of the beam only without the spring and mass. In other words, the attached spring and mass decreased the first natural frequency of the beam.

The vibrational frequency in water is generally much lower than that in air because of the added mass effect. A previous experimental study [18] showed that an E-glass composite cantilever beam has a reduction in frequency by 70 % due to water. In other words, the frequency in water is 30 % of that in air. Metallic beams have smaller reduction in natural frequency because of a smaller FSI effect. Such reduction depends on the boundary condition and the material properties. Unfortunately, it is not easy to construct the structural mass matrix including the added mass due to FSI so as to compute the natural frequency in water using the eigenvalue analysis. Instead, a numerical modal analysis was conducted to the composite beam as well as the composite system as described below.

A short duration of impulse was applied to a location in the beam structure, and the dynamic response is determined at various locations as a function of time. For example, displacements,

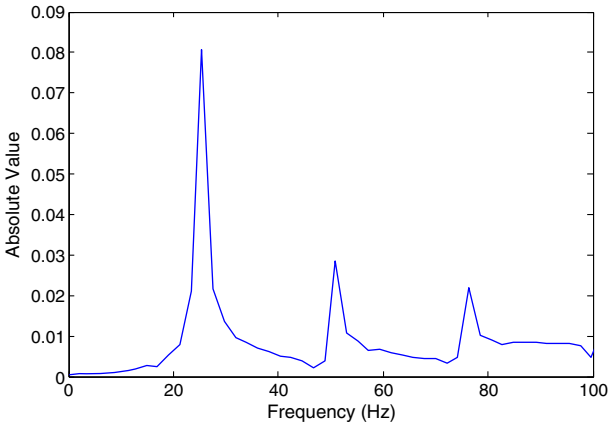

Fig. 7 FFT plot of clamped composite beam submerged in water with centrally attached mass and spring

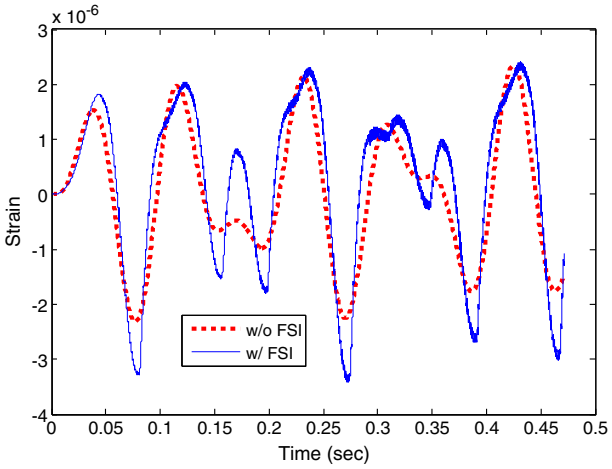

Fig. 8 Strain at the center element for clamped composite beam subjected to 10 Hz vibrating force

velocities and/or accelerations can be computed. For the experimental modal analysis, accelerometers are mostly used because they are compact and easy to measure. However, for the numerical modal analysis, there is no such a difference. As a result, the time history of a displacement was used for the present study. Then, the Fast Fourier Transform (FFT) was conducted to convert the time domain response to the frequency domain data to determine the natural frequencies.

For the present clamped composite beam without the spring and mass, an impulse was applied to near the center of the beam, and the center displacement was obtained for FFT. Figure 6 shows the FFT of the displacement. From the graph, the first natural frequency of the clamped composite beam submerged in water is 16 Hz which is approximately one fourth of the frequency in air.

The same numerical modal analysis was conducted for the clamped composite beam in water with centrally attached mass and spring in order to find the natural frequency. Figure 7 shows the FFT plot with the first three natural frequencies of 25 Hz, 51 Hz, and 76 Hz,

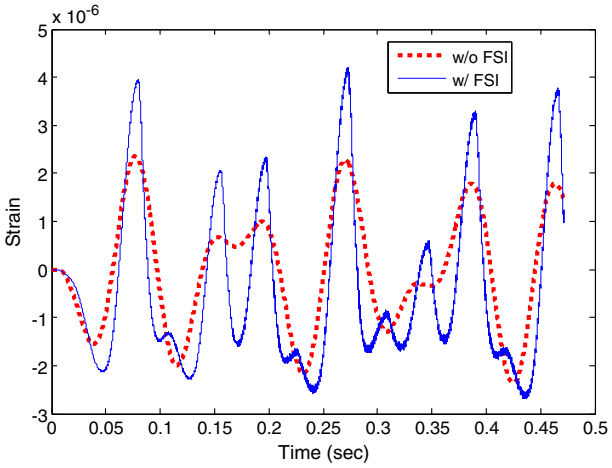

Fig. 9 Strain at the boundary element for clamped composite beam subjected to 10 Hz vibrating force

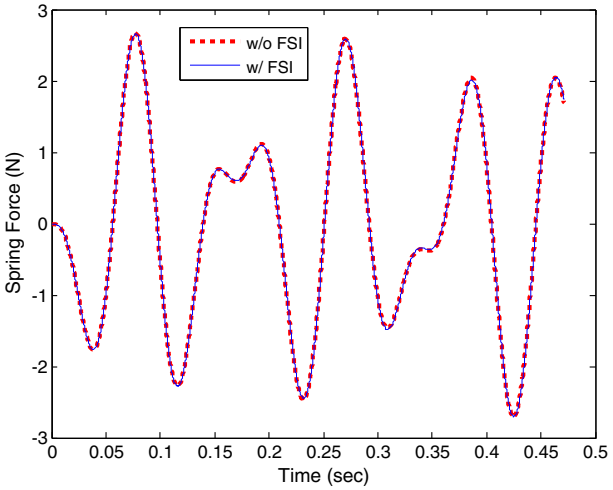

Fig. 10 Spring force for clamped composite beam subjected to 10 Hz vibrating force

respectively, for $\sqrt{K/M} = 100\ (1/\text{sec})$. This ratio of $\sqrt{K/M}$ was selected because it resulted in the first natural frequency of the dry composite beam system as 16 Hz like the wet composite beam. The first natural frequency of the wet composite beam increased with the attached spring and mass while the second natural frequency was reduced from 187 Hz.

When selecting values for the singles mass M and spring M, the force transmissibility was considered. Assuming the rigid base structure, the force transmissibility (TR) is expressed as below without damping

$$TR = \frac{1}{1-r^2} \tag{30}$$

where $r=\omega/\omega_n$ and ω is the applied frequency while $\omega_n = \sqrt{K/M}$. To consider the largest force transmission to the structure as the worst case, the frequency ratio r should be very small

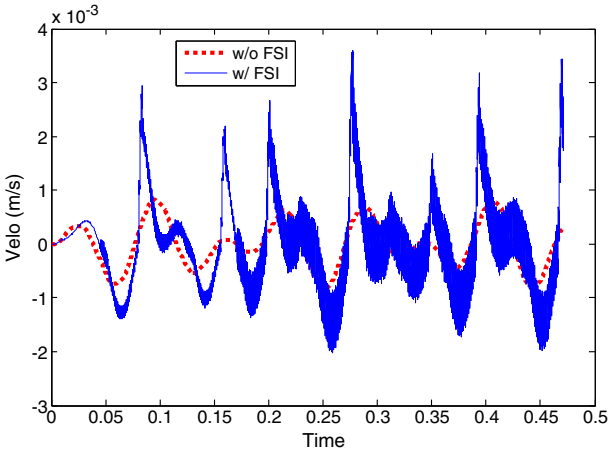

Fig. 11 Velocity at the center for clamped composite beam subjected to 10 Hz vibrating force

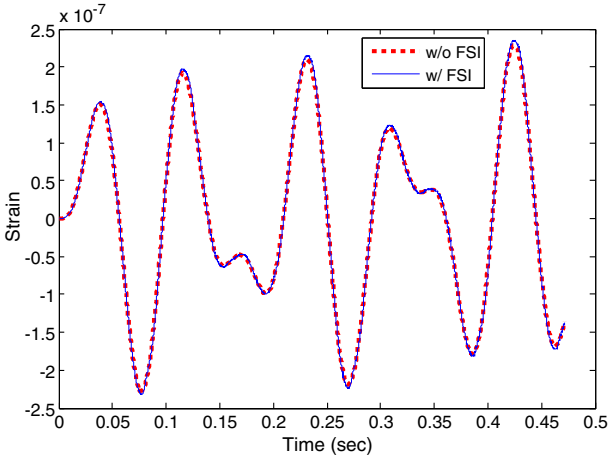

Fig. 12 Strain at the center for clamped steel beam subjected to 10 Hz vibrating force

compared to the unity. That means ω_n should be much greater than ω. With ω_n chosen to be 100 Hz, the vibrational frequency ω was set to 10 Hz which is lower than the first natural frequencies for all the cases studied above for the clamped composite beam. All the plots below are normalized for the unit value of force, i.e., F_o=1 N.

With the selected values, the composite beam was first analyzed. The bending strain at the center of the beam was computed for the composite beam, and its time history is plotted in Fig. 8. Likewise, the bending strain at the boundary is also plotted in Fig. 9. The bending strains were computed on the side in contact with water. Because the curvature in a clamped beam is opposite between the center and the boundary, the bending strains show opposite signs in Figs. 8 and 9. Without the FSI effect, the magnitudes of the bending strains at both elements are similar. The FSI effect with water significantly increases the bending strains in the composite beam. The bending strain at the boundary was more influenced by FSI than that at the center. The maximum peak strain was increased by approximately 50 % at the center and

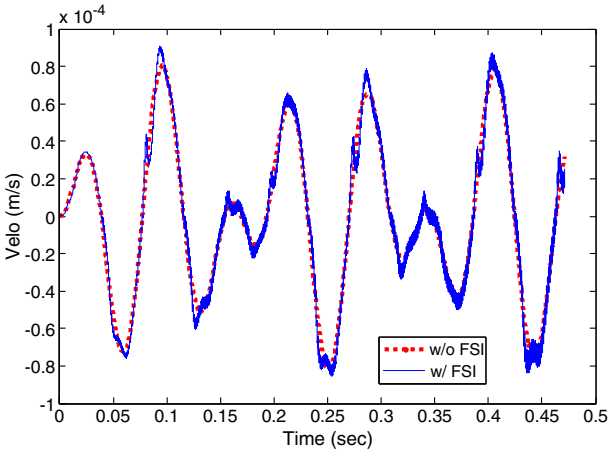

Fig. 13 Velocity at the center for clamped steel beam subjected to 10 Hz vibrating force

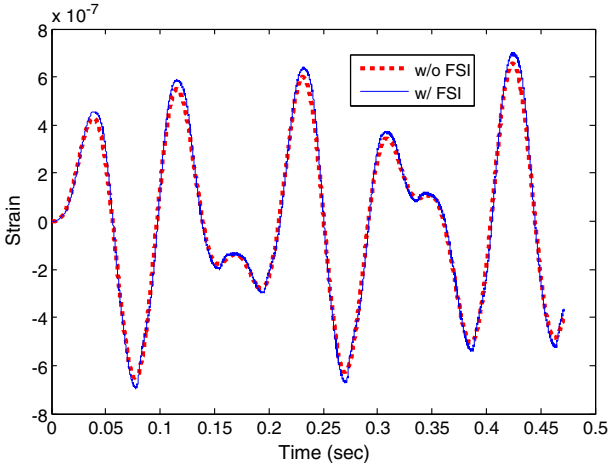

Fig. 14 Strain at the center for clamped aluminum beam subjected to 10 Hz vibrating force

85 % at the boundary. Additionally, the variation in peaks and valleys of the strain history is more profound with FSI. The result clearly suggests that the FSI effect on the composite beam in contact with water will significantly reduce the fatigue life of the structure.

In order to further understand the FSI effect, the force induced in the spring was plotted in Fig. 10. The figure shows that the force in spring was not affected by the FSI. There is no change in the force because of FSI. On the other hand, the velocity at the center of the composite beam is plotted in Fig. 11. The velocities with and without the effect of the FSI are drastically different. Interestingly the plot of central deflection of the beam was very similar to the strain plot at the center element as shown in Fig. 8. Therefore, the deflection plot is omitted here.

Under the same condition, both steel and aluminum beams were also tested, and their responses are shown in Figs. 12, 13, 14 and 15. The steel beam has almost no FSI effect on both the bending strain and velocity as seen in Figs. 12 and 13. Likewise, the aluminum beam also has a negligible FSI effect on the bending strain as shown in Fig. 14. As far as the central

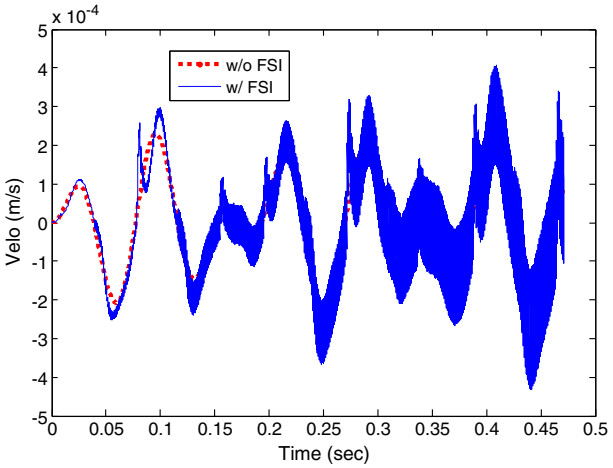

Fig. 15 Velocity at the center for clamped aluminum beam subjected to 10 Hz vibrating force

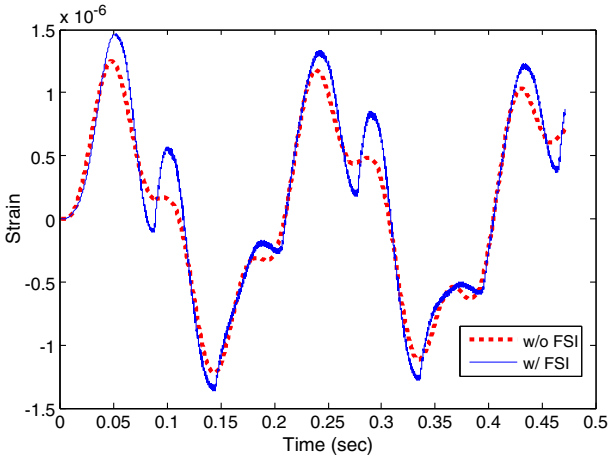

Fig. 16 Strain at the center for clamped composite beam subjected to 5 Hz vibrating force

velocity is concerned, the time-history is very close between with and without FSI in terms of the phase and magnitude. However, FSI induced additional very high frequency responses in the velocity of the aluminum beam like the composite beam. Such a high frequency response was also observed during the free vibrational experiment of a composite cantilever beam [18].

Comparing the three different materials, the composite beam showed the much largest FSI effect because of its lower density and stiffness. In the next study, some of the parameters in the system were varied to determine what parameter yields the most critical FSI effect. First of all, the equipment vibrating frequency was changed from 10 Hz to 5 Hz. Comparing Figs. 16, 17 and 18 suggests that the lower vibrating frequency results in a little less FSI effect on the bending strain at the beam center. This is because 10 Hz is closer to the natural frequency of the composite beam in water.

In order to further investigate the effect of the exciting vibrational frequency on the dynamic response of the composite beam, the vibrational frequency was changed gradually and the ratio of the maximum dynamic deflection to the static deflection at the center of the

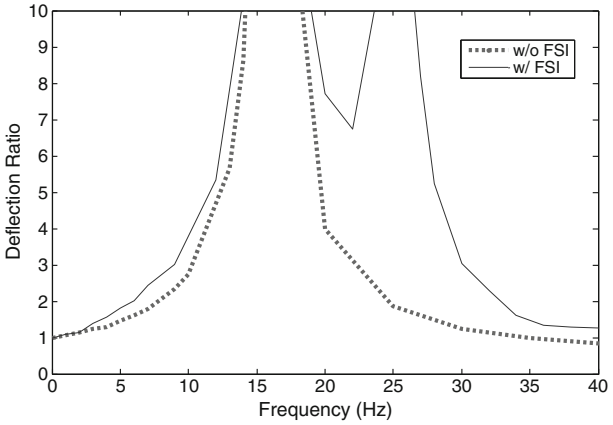

Fig. 17 Plot of deflection ratio as a function of the exciting vibrational frequency

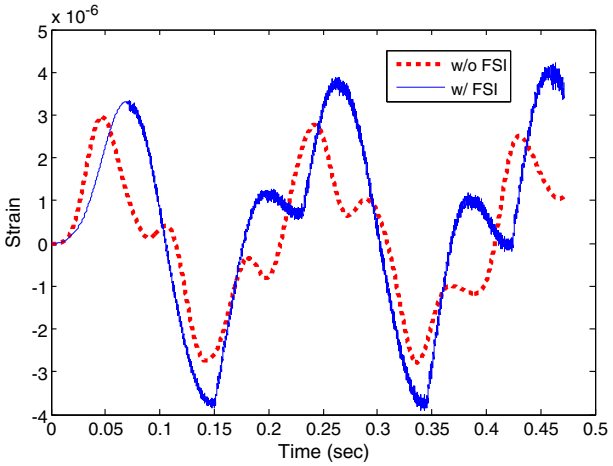

Fig. 18 Strain at the center for simply supported composite beam subjected to 5 Hz vibrating force

clamped composite beam was computed as plotted in Fig. 17. The figure shows two resonance frequencies for the beam submerged in water and one resonance frequency for the dry beam up 40 Hz. Those resonance frequencies agree with the natural frequencies discussed previously. Comparing the deflection ratios between with and without FSI shown in Fig. 17 clearly suggests that the FSI effect significantly increases the deflection of the composite beam, i.e., the greater bending strains.

The following study changed the boundary condition of the beam. The beam was simply supported instead of clamped. The vibrating frequency was 5 Hz in order to be much lower than its natural frequency in water for the simply supported beam. Bending strains at the center and the boundary are plotted in Figs. 18 and 19. The more flexible boundary such as simply supports yields a much larger difference between the strains with and without the FSI effect. Such a difference is more profound at the simply supported boundary as seen in Fig. 19. The

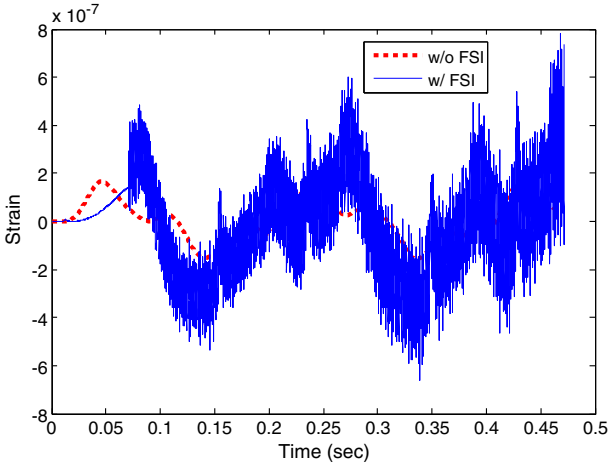

Fig. 19 Strain at the boundary for simply supported composite beam subjected to 5 Hz vibrating force

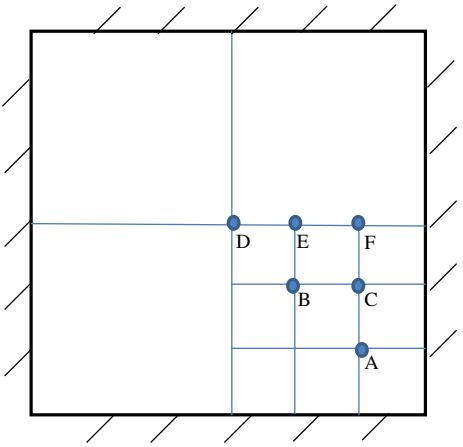

Fig. 20 Locations on the clamped plate where displacements were compared between dry and wet vibrations

FSI effect resulted in the bending strain nearly three times greater at the boundary along with very high frequency components in the strain-time history.

Finally, a clamped composite plate was also studied. The material is the same E-glass composite as used for the beam, and its dimension is 1 m × 1 m and 0.02 m thick. The vibrating equipment was located at the center of the square plate with the same single mass and spring ratio of $\sqrt{K/M} = 1000$ (rad/sec) as before. The first natural frequency of the dry composite plate without the single mass and spring was computed from the following formula

$$\omega_n = 1.655\sqrt{\frac{Eh^2}{\rho L^4(1-\nu^2)}}(\text{Hz}) \tag{31}$$

where E and ν are the elastic modulus and Poisson's ratio, ρ is the volume density, and L and h are the length and thickness of the square plate. The natural frequency of the dry plate without the single mass and spring is 110 Hz from Eq. (31). When the spring and mass were included, the natural frequency was computed form the eigenvalue analysis of the finite element model and it becomes 16 Hz. The natural frequency of the plate in contact with water was also computed using the numerical modal analysis, and the frequency is 36 Hz. As a result, the exiting frequency of the equipment was selected as either 10 Hz or 20 Hz.

The transverse displacement was computed at multiple locations on the plate and compared between the dry and wet vibrations. The selected locations are shown in Fig. 20. The ratio of

Table 3 Ratio of maximum displacement between the wet and dry clamped composite plate (Please see Fig. 20 for the location)

Location	Excitation frequency	
	10 Hz	20 Hz
A	1.20	1.41
B	1.14	1.31
C	1.16	1.34
D	1.11	1.24
E	1.14	1.29
F	1.16	1.33

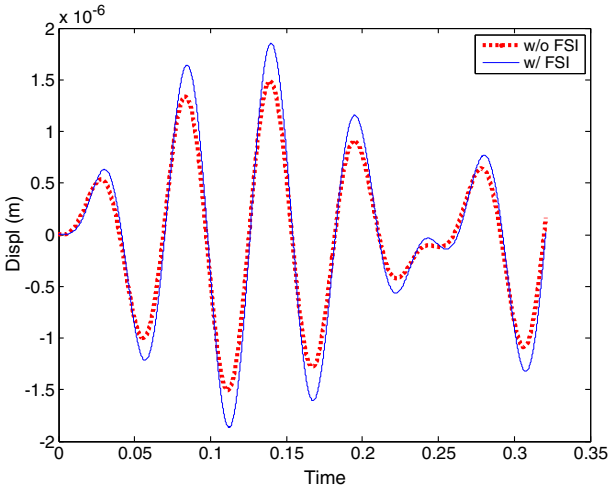

Fig. 21 Displacement at the center of clamped composite plate subjected to 20 Hz vibrating force

the maximum transverse displacement of the wet plate to the dry plate is listed in Table 3 for two different excitation frequencies, respectively. The results showed that the largest difference between the wet and dry plate deflections occurs at location A in Fig. 20 while the least difference occurs at location D. This data suggests that the FSI effect is larger at a location closer to the clamped boundary and smaller at a location nearer to the plate center. This statement can also be confirmed by comparing the locations B and C, as well as the locations D, E, and F, respectively. At location A close to the boundary corner, the displacement of the wet plate was 20 % and 41 % greater than that of the dry plate for the two different excitation frequencies. The vibrating equipment with 20 Hz resulted in more than a 40 % increase in the deflection at location A. The transverse displacement at the center of the plate is plotted in Fig. 21 to illustrate the vibrational motion of the plate.

6 Conclusions

Dynamic responses of polymer composite beam and plates were examined using a multiphysics modeling technique when the structures supported vibrating equipment on one side and they were in contact with water on the other side. This is the common case for a ship hull structure. The coupled FEM and CA techniques were used for the study. The effect of FSI along with the harmonic excitation influenced the composite structural response. As the displacement, velocity, acceleration, and strain were compared between the same composite structures in air or water, respectively, the FSI increased their magnitudes noticeably throughout a range of excitation frequencies. In other words, design and analysis of composite structures to support any vibrating machinery would be non-conservative if the effect of FSI were not considered properly when the structure is in contact with water. On the other hand, the effect of FSI was much smaller for metallic structures made of either aluminum or steel. The effect of FSI along with the harmonic excitation was greater for a simply supported boundary than a clamped boundary. For a composite plate, the FSI effect was larger at a location close to the boundary and smaller at a location near to the plate center.

Acknowledgments This work is supported by Office of Naval Research (ONR) Solid Mechanics Program. The Program Manager is Dr. Yapa Rajapakse. The financial support is greatly appreciated.

References

1. Nilsson, A.C.: Wave propagation in simple hull-frame structures of ship. J. Sound Vib. **44**(3), 393–405 (1976)
2. Skaar, K.T., Carlsen, C.A.: Modelling aspects for finite element analysis of ship vibration. Comput. Struct. **12**(4), 409–419 (1980)
3. Wu, J.-S., Sheu, J.J.: An exact solution for a simplified model of the heave and pitch motions of a ship hull due to a moving load and a comparison with some experimental results. J. Sound Vib. **192**(2), 495–520 (1996)
4. Noonan, E.F., Feldman, S.: State of the art for shipboard vibration and noise control. Ship Vibration Symposium. The Society of Naval Architecture and Marine Engineering, Arlongton, Virginia, October 1978
5. Carlton, J.S., Vlasic, D.: Ship vibration and noise: Some topical aspects. 1st Int. Ship Noise and Vibrational Conference, London, June 2005
6. Cho, D.-S., Lee, S.-M., Chung, K.-Y.: Ship vibration control using a force-adjustable mechanical actuator. J. Vib. Control. **5**, 779–794 (1999)
7. Gray, L.M., Greeley, D.S.: Source level model for propeller blade rate radiation for the world's merchant fleet. J. Acoust. Soc. Am. **67**(2), 516–522 (1980)
8. Kwon, Y.W., Fox, P.K.: Underwater shock response of a cylinder subjected to a side on explosion. Comput. Struct. **48**(4), 637–646 (1993)
9. Kwon, Y.W., Bergensen, J.K., Shin, Y.S.: Effect of surface coatings on cylinders exposed to underwater shock. J. Shock Vib. **1**(3), 637–646 (1994)
10. Faltinsen, O.M.: Hydroelastic slamming. J. Mar. Sci. Technol. **5**(2), 49–65 (2000)
11. Marshall, B.R.: A surface navy vibration program over view: standardization and state-of-the-art. Nav. Eng. J. **100**(3), 90–100 (1988)
12. Hylarides, S., Vorus, W.S.: The added mass matrix in ship vibration, using a source distribution related to the finite element grid of the ship structure. Int. Shipbuild. Prog. **29**(330), 1–16 (1982)
13. Wilken, M., Of, G., Cabos, G., Steinback, O.: Efficient calculation of the effect of water on ship vibration. In: Soares, C.G., Das, P.K. (eds.) Analysis and Design of Marine Structures. Taylor and Francis Group, London (2009)
14. Jennings, A.: Added mass for fluid-structure vibration problems. Int. J. Numer. Methods Fluids **5**(9), 817–830 (1985)
15. Kwon, Y.W., Violette, M.A., McCrillis, R.D., Didoszak, J.M.: Transient dynamic response and failure of sandwich composite structures under impact loading with fluid structure interaction. Appl. Compos. Mater. **19**(6), 921–940 (2012)
16. Kwon, Y.W., Violette, M.A.: Damage initiation and growth in laminated polymer composite plates with fluid-structure interaction under impact loading. Int. J. Multiphys. **6**(1), 29–42 (2012)
17. Craugh, L.E., Kwon, Y.W.: Coupled finite element and cellular automata methods for analysis of composite structures with fluid-structure interaction. Compos. Struct. **102**, 124–137 (2013)
18. Kwon, Y.W., Priest, E.M., Gordis, J.H.: Investigation of vibrational characteristics of composite beams with fluid-structure interaction. Compos. Struct. **105**, 269–278 (2013)
19. Kwon, Y.W., Hosoglu, S.: Application of Lattice Boltzmann method, finite element method, and cellular automata and their coupling to wave propagation problems. Comput. Struct. **86**(7–8), 663–670 (2008)
20. Kwon, Y.W.: Analysis of laminated and sandwich composite structures using solid-like shell elements. Appl. Compos. Mater. **20**(4), 355–373 (2013)